Available online at www.sciencedirect.com
SCIENCE DIRECT®
PERGAMON
Deep-Sea Research I 50 (2003) 917–926
DEEP-SEA RESEARCH PART I
www.elsevier.com/locate/dsr

# Forced Rossby wave in the northern South China Sea

Haijun Yang[a,*], Qinyu Liu[b]

[a] Department of Atmospheric Science, Peking University, Beijing, China
[b] Physical Oceanography Laboratory, Ocean University of China, Qingdao, China

Received 26 February 2002; accepted 7 April 2003

**Abstract**

Time-longitude diagrams of monthly anomalies of TOPEX/Poseidon sea surface height (SSH), Levitus steric height, COADS wind stress curl, as well as meridional surface wind averaged over the northern South China Sea (SCS) from 18° to 22°N, exhibit a coherent westward phase propagation, with a westward propagation speed of about 5 cm $s^{-1}$. The consistency between oceanic and atmospheric variables indicates that there is a forced Rossby wave in the northern SCS. The horizontal patterns of monthly SSH anomalies from observations and model sensitivity experiments show that the forced Rossby wave, originating to the northwest off Luzon Island, actually propagates west-northwestward towards the Guangdong coast because of zonal migration of the meridional surface wind. The winter Luzon Cold Eddy (LCE), which has been found from field observations, can be identified as a forced Rossby wave with a negative SSH anomaly in winter. It corresponds to strong upwelling and a negative temperature anomaly. Sensitivity experiments show that the wind forcing controls the generation of the LCE, while the Kuroshio is of minor importance.


*Keywords:* South China Sea; Rossby wave; Luzon cold eddy

## 1. Introduction

The South China Sea (SCS) is the largest marginal sea in Southeast Asia, with a total area of 3.5 million $km^2$ and an average depth of over 2000 m (Fig. 1). It is a semi-enclosed basin that exchanges waters with the western Pacific, mainly through the Luzon Strait. The climate of the SCS belongs to the Southeast Asia monsoon system (Wyrtki, 1961). The upper ocean circulation within the SCS has a dramatic seasonal variability driven by the SCS monsoon wind (Wyrtki, 1961; Shaw and Chao, 1994; Chu et al., 1999; Liu et al., 2001). Observations from TOPEX/Poseidon (T/P) altimetry (Chambers et al., 1997; Shaw et al., 1999; Ho et al., 2000) and numerical studies (Shaw and Chao, 1994; Chao and Shaw, 1996; Chu et al., 1999; Yang et al., 2002) indicate that the basin-scale circulation of the upper SCS is generally cyclonic in the winter, in accordance with the northwesterly monsoon, reversing to anticyclonic in the summer due to the monsoon reversal. The adjustment in SCS upper circulation to the changing monsoon can be understood in terms of Rossby wave dynamics (Liu et al., 2001). The SCS upper circulation is always in a quasi-steady response under an annual forcing due to the short

*Corresponding author. Center for Climatic Research, University of Wisconsin–Madison, 1225 W. Dayton St., Madison, WI 53706-1695, USA.
*E-mail address:* haijunyang@wisc.edu (H. Yang).

0967-0637/03/$ - see front matter 
doi:10.1016/S0967-0637(03)00074-8

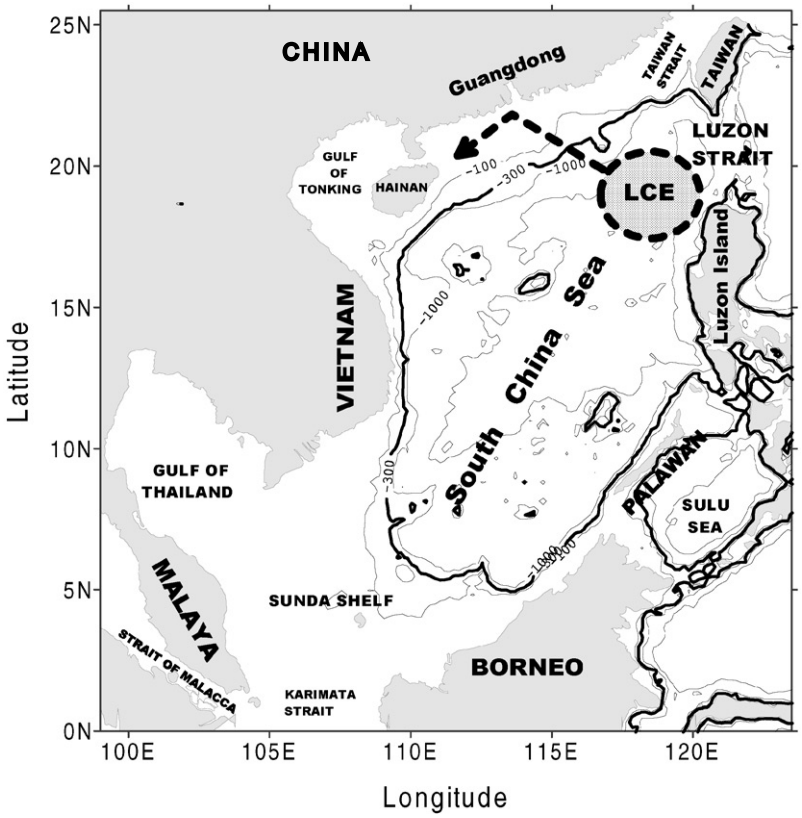


Fig. 1. Bathymetry of the South China Sea (SCS). The 300 m isobath is indicated by the thick solid line. The thick dashed circle represents the LCE with the direction of movement indicated by the thick dashed arrow.

thermocline adjustment time. The forced baroclinic Rossby wave plays a critical role in the adjustment of SCS upper circulation.

The westward wave propagation can be seen only in the very northern part of the SCS. South of 18°N, the sea surface height anomalies (SSHA) obtained from T/P altimetry and steric height calculated from Levitus monthly climatology exhibit eastward zonal migration, which appear to be forced by eastward migration of wind stress curl (Liu et al., 2001). The regional dynamics of the SCS circulation south of 18°N has been discussed in detail in Liu et al. (2001). North of 18°N, the T/P SSHA shows a distinctly westward phase propagation, which is also seen in an upper oceanic thermocline anomaly, the atmospheric wind stress curl, and the meridional surface wind anomaly. The coherent westward propagation in both oceanic and atmospheric variables suggests that there exists a forced baroclinic Rossby wave in the northern SCS.

In this paper, the observational evidence for a forced Rossby wave in the northern SCS is presented. Using the Princeton Ocean Model (POM), we reproduce the forced Rossby wave and further explore the mechanism of its generation and evolution. Both the observations and modeling show that this forced wave does not propagate purely westward but instead west-northwestward. It has a 1-year period and exhibits a negative (positive) SSHA northwest off Luzon Island during winter (summer). Model sensitivity experiments demonstrate that the west-northwestward migration of the forced Rossby wave is caused by wind forcing. Without wind forcing, the forced response in the northern SCS would be

reduced significantly and eventually migrate west-southwestward.

The winter Rossby wave forced by the winter monsoon can be associated with the Luzon Cold Eddy (LCE) northwest off the Luzon Island. As argued below, the LCE can be understood in terms of a forced Rossby wave. The LCE (Fig. 1) has been well identified from many oceanic investigations of the SCS (e.g., Guo, 1988; Shaw et al., 1996; Yang and Liu, 1998; Qu, 2000). It is characterized by a cold-water center with temperatures lower than 20°C and corresponds to strong upwelling. However, the formation mechanism and three-dimensional structure of the LCE have not yet been clearly explored. We found that the LCE corresponds to the negative phase of a forced Rossby wave originating off northwestern Luzon Island. The evolution process of the LCE is therefore predominately controlled by wind stress curl over the northern SCS.

## 2. Data and model

Altimeter observations from the T/P mission (Chambers et al., 1997) were used to extract the Rossby wave signal in the northern SCS and also to provide comparison with model SSH. The T/P altimetry data from 1992 to 1998 was composed into a monthly climatology. The data was corrected for all media and instrument effects (ionosphere, wet and dry troposphere, and electromagnetic bias) and geophysical effects (tides and inverted barometer) (Chambers et al., 1997). A gridded/smoothed version ($1^\circ \times 1^\circ$ resolution) compiled by the Center for Space Research, University of Texas, was used. The spatial filter used for the data is a rectangular Gaussian-squared filter spanning 1000 km in longitude and 450 km in latitude. The T/P data, with the nearest track 200 km away, may not capture small-scale features realistically, but it should be reasonably adequate for basin-scale features in the SCS, as shown recently by Shaw et al. (1999).

Monthly climatologies of Levitus temperature and salinity (Levitus and Boyer, 1994) were used to calculate the steric height of the SCS and serve as the initial condition in the numerical model (POM) as well. COADS (da Silva et al., 1994a) monthly wind stress was used to illustrate the time-longitude structure of the wind field over the SCS and also to force the model (Fig. 2). The detailed configuration of the POM used in this paper can be found in Yang et al. (2002). It has a realistic topography and a free surface (Blumberg and Mellor, 1987). The model's domain includes almost the entire Pacific, ranging from 20°S to 45°N and from 98°E to 70°W; containing the SCS, the Pacific Ocean, and most of the Japan Sea. Non-uniform horizontal resolution is used here. Within the SCS (0°–30°N, 98°E–125°E), the grid interval is $0.5^\circ \times 0.5^\circ$ in both meridional and zonal directions. Outside of the SCS, from the SCS boundaries to model boundaries, the grid interval increases linearly from 0.5° to 2° and from 0.5° to 5° in the meridional and zonal directions,

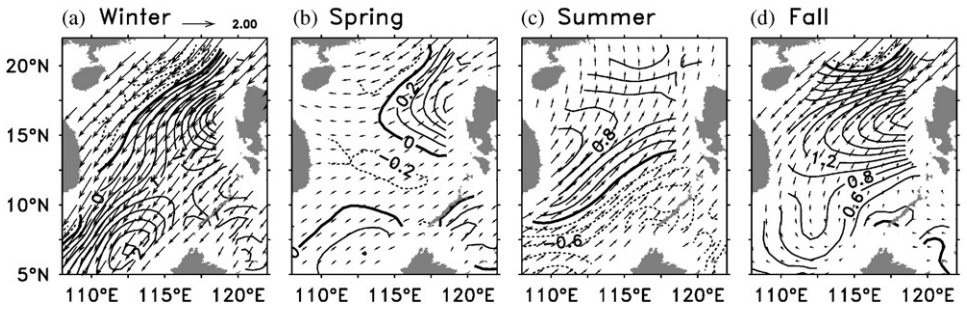


Fig. 2. Seasonal mean COADS wind stress $\tau/\rho_0$ (vectors, $10^{-5}\,m^2\,s^{-2}$) and wind stress curl $curl(\tau/\rho_0)$ for (a) winter (December–February), (b) spring (March–May), (c) summer (June–August) and (d) fall (September–November). $\rho_0$ is the sea water density. Contour interval (CI) is $0.2 \times 10^{-10}\,m\,s^{-2}$.

Table 1
Scheme of four POM experiments

| Experiments | Scheme |
|---|---|
| EXP1 (control) | All external forcing included |
| EXP2 (no-heat) | No buoyancy forcing |
| EXP3 (no-wind) | No wind forcing |
| EXP4 (no-open) | Closing all straits |

respectively. The model boundary condition is no-normal flow condition. The model has 15 vertical sigma levels so that the total model grid points are $116 \times 90 \times 15$. The minimum and maximum depth for the model are 10 and 4500 m.

The POM was initialized with the annual mean Levitus temperature and salinity. The surface heat flux was calculated as restoring towards the climatological annual cycle of SST, using a restoring coefficient determined from COADS data (da Silva et al., 1994a). The surface salinity flux was calculated with the E−P (evaporation minus precipitation) climatology from COADS (da Silva et al., 1994a). The model was run for 10 years starting from the same initial state for all experiments, of which the last 5 years of the simulation were composed into a seasonal cycle. The upper SCS circulation quickly reaches equilibrium state in 2–3 years due to the basin's relatively small size (Liu et al., 2001). One control run (EXP1) and three sensitivity experiments were carried out to address the individual effects of wind forcing, buoyancy forcing and the Kuroshio on the SCS circulation (Table 1).

## 3. Horizontal evolution of SSH

### 3.1. Westward propagation

The observations from T/P SSH and Levitus steric height clearly show the westward phase propagation in the northern SCS (Figs. 3a and b). The SSH anomaly (SSHA) was first averaged between 18°N and 22°N, and then the zonal mean SSHA was removed for each month (White, 2000, 2001; Liu et al., 2001). The zonal gradient of SSH, that is, the meridional geostrophic current of the upper ocean, remains undistorted throughout the seasonal cycle. There are three remarkable features in Figs. 3a and b. First of all, the westward propagating Rossby wave is clearly illustrated. This wave appears to originate in the east and propagate westward with decreasing amplitude. Second, there are two abrupt phase reversals of the Rossby wave: the first reversal occurs during April and May with the SSHA reversing from negative to positive; the second one occurs during September and October with the SSHA changing from positive to negative. Third, the Rossby wave has a nearly annual period, with both the positive and negative phases lasting about 6 months. Figs. 3a and b have similar patterns and comparable amplitude as well, although these two data sets are completely independent. The heat content anomaly over the upper ocean (0–300 m) from Levitus data (Fig. 3c) also clearly demonstrates the westward propagating Rossby wave with a similar pattern; positive (negative) SSHA corresponds to a warmer (colder) upper ocean. They are physically consistent, and the similarity of Figs. 3a–c suggests the robustness of the westward Rossby wave in the northern SCS.

This annual cycle of the westward Rossby wave appears to be controlled mainly by the westward migration of wind stress curl, or, more precisely, meridional surface wind. Figs. 3d and e also exhibit the feature of westward phase propagation in wind stress curl and meridional wind. A positive wind stress curl anomaly generates Ekman upwelling in winter and cools the upper ocean (Fig. 3c), causing a negative SSHA (Figs. 3a and b), while the opposite occurs in summer. The wind stress curl anomaly is determined mainly by the zonal gradient of meridional surface wind anomaly (Fig. 3e). The phase reversal of wind stress curl anomaly is actually the result of the transition of the meridional monsoon wind. The SCS monsoon wind belongs to the planetary scale atmospheric systems such as South Asian monsoon, which is minimally affected by the SCS oceanic circulation. Therefore, the northern SCS oceanic variability is a sort of forced response in terms of the westward Rossby wave. The forced Rossby wave experiences abrupt phase reversal during spring (April and May) and fall (September and October) due to the

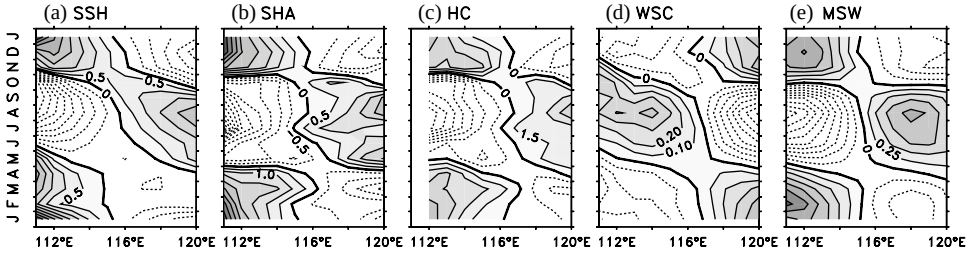


Fig. 3. Time-longitude plots of seasonal anomalies of (a) TOPEX/Poseidon SSH, (b) Levitus steric height, (c) upper ocean heat content from surface to 300 m depth, (d) wind stress curl and (e) meridional surface wind. All variables are averaged over the northern SCS (18°–22°N) with zonal mean removed. Contour intervals are 0.5 cm for (a) and (b), $1.5\times10^{8}\,\mathrm{J\,m^{-2}}$ for (c), $0.1\times10^{-10}\,\mathrm{m\,s^{-2}}$ for (d) and $0.25\times10^{-6}\,\mathrm{m^{2}\,s^{-2}}$ for (e).

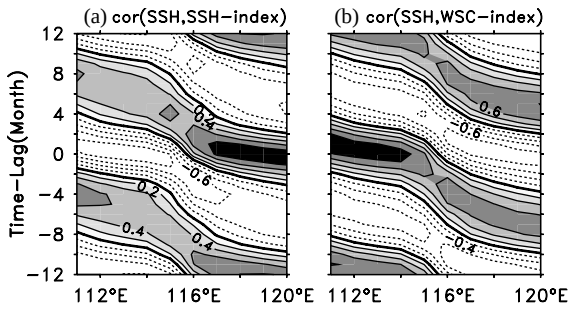


Fig. 4. Lag correlations between (a) SSH and eastern SCS SSH index from T/P altimetry, and between (b) T/P SSH and eastern SCS wind stress curl index. The data used here are extended to 3 years that includes three identical seasonal cycles, to facilitate a maximum 12-months lag correlation. The T/P SSH index and wind stress curl index are obtained by zonally averaging SSH and wind stress curl between 117° and 120° E. The CI is 0.2 for both (a) and (b).

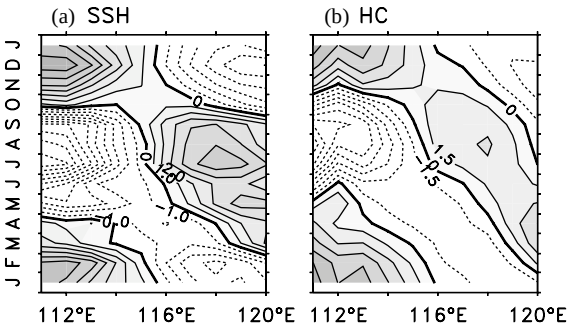


Fig. 5. Time-longitude plots of seasonal anomalies for (a) simulated SSH and (b) heat content over upper 300 m. All variables are averaged over the northern SCS (18°–22°N) with zonal mean removed. Contour intervals are 1 cm for (a) and $1.5\times10^{8}\,\mathrm{J\,m^{-2}}$ for (b).

sudden transition of the monsoon system. Also, this forced Rossby wave has an annual cycle because of the annual period of the monsoon wind.

Lag correlation between SSH and eastern SCS SSH index based on T/P data (Fig. 4a) further illustrates the westward propagating Rossby wave, and the lag correlation between T/P SSH and eastern SCS wind stress curl index (Fig. 4b) suggests that this Rossby wave results from wind stress forcing. The data used here are extended to 3 years that include three identical seasonal cycles to facilitate a maximum 12-months lag correlation. The T/P SSH index and wind stress curl index were obtained by zonally averaging SSH and wind stress curl within 117–120° E. Fig. 4a shows that the anomalous signals, which always appear first in the eastern SCS and reach the western boundary 6–8 months later with reduced amplitude, yield a westward phase speed of about $5.3\pm1.0$ cm/s, which is within the range of estimation by White (2001) for the ocean between 10°N and 26°N.

Numerical modeling successfully captures the westward phase propagation features as shown in observations (Fig. 3). Fig. 5 shows the simulated SSH and upper ocean heat content. The modeled SSH and heat content anomalies demonstrate similar westward propagating Rossby wave, along with the timing of the phase reversal and the period. The correlations between modeling and observation are greater than 0.8 for both the SSH and upper ocean heat content. Other detailed comparisons between modeling and observations have been made by Liu et al. (2001) and Yang et al.

(2002). The model reproduces the upper circulation in the SCS quite well, although the simulated SSH (Fig. 5a) has an amplitude larger than that observed (Fig. 3a). This validates the model for further sensitivity studies of the northern SCS circulation. In the next section, the horizontal structure of the northern SCS circulation will be discussed in detail.

### 3.2. Horizontal patterns

The evolution of the SSH in the northern SCS manifests the westward propagating forced Rossby wave originating from northwest Luzon Island, where the Rossby wave is easily excited because of strong local wind forcing (Fig. 2) and the Kuroshio Loop Current in the Luzon Strait (Liu and Liu, 1996). Figs. 6a and b show that the forced Rossby wave propagates northwestward with decreasing amplitude. It is captured by the coast once it reaches the western boundary and transforms into a coastal Kelvin wave that rapidly propagates southward. In all the figures, the annual mean SSH has been removed. The first column (Fig. 6a) depicts the T/P SSHA, and the second column represents the model control run (EXP1) (Fig. 6b). The correlation between EXP1 SSHA and T/P SSHA is greater than 0.6 (Yang et al., 2002). The negative SSHA, that is, the negative forced Rossby wave in Figs. 6a and b, represents the LCE, which has been identified from observations (Guo, 1988; Shaw et al., 1996; Yang and Liu, 1998; Qu, 2000). The control run (Fig. 6b) shows that the fully developed LCE occurs in January with a center value of −12 cm located at 19.5°N, 118°E. In February, the LCE is slightly weaker, with a smaller horizontal scale and amplitude of −10 cm, and moving westward towards 19.5°N, 117°E. In March, the LCE shrinks and moves further northwestward with the center rising to −6 cm. In April, the low center reaches the Guangdong coast. Although the contours of low SSHA are still moving cyclonically, there is no longer a closed cyclonic eddy. Now the LCE has completely disappeared. At the same time, a positive SSHA appears off northwestern Luzon Island, occupying the place of the winter LCE. This positive SSH gradually forms an anticyclonic eddy during May and June and finally becomes a closed eddy in July. It is obvious that the SSH in July is exactly out of phase with that in January. During August and September, the anticyclonic eddy, similar to the winter LCE, also moves northwestward with decreasing amplitude. In October, the positive SSH disappears completely, and the negative SSH reappears northwest off Luzon Island. In November, the negative SSH expands northwestward, finally forming a closed cyclonic eddy, the LCE, in December.

The horizontal evolution of the northern SCS SSH is also clearly identified from T/P altimetry (Fig. 6a) despite the relatively coarse resolution. Both observations and the model suggest an annual cycle for the northern SCS SSH as previously described. The SSHAs in January and February are out of phase with those in July and August, respectively. The life span of the LCE is about 6 months, from October to the following March.

One significant feature that should be highlighted in Fig. 6b is that the forced Rossby wave, and therefore the LCE, does not propagate purely westward but west-northwestward, which results from the zonal migration of the meridional surface wind. Further evidence from sensitivity experiments is provided next to show the relative role of the wind forcing, buoyancy forcing and inflow through the Luzon Strait.

### 3.3. Mechanism

Three sensitivity experiments were conducted to explore the individual contributions of the wind forcing, surface buoyancy forcing, and mass transport through SCS straits to the forced Rossby wave in the northern SCS. It bears noting that, at the zeroth order approximation, the northern SCS circulation can be thought of as a linear superposition of the effects from the wind forcing, surface buoyancy forcing, and incoming mass transport through the straits (e.g., the Luzon Strait, the Taiwan Strait and even the Karimata Strait), while the non-linear effects resulting from the interactions among these three factors on the northern SCS circulation can be ignored. In these sensitivity experiments, the buoyancy forcing is

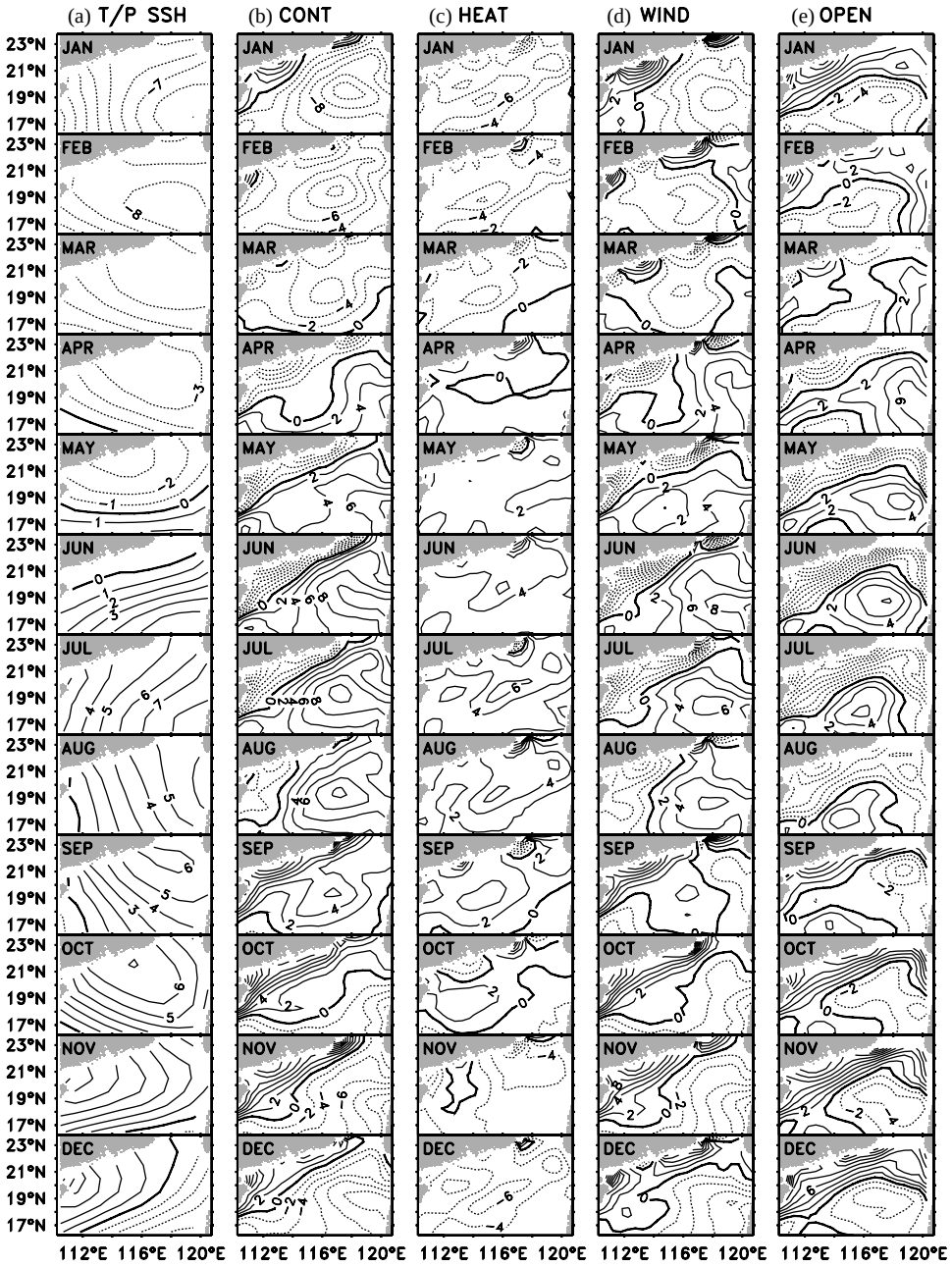


Fig. 6. The monthly SSH anomalies in the northern SCS from (a) TOPEX/Poseidon altimetry and (b–e) model experiments, respectively, (b) the control run, (c) the buoyancy forcing run, (d) the wind forcing run and (e) the open boundary forcing run. CI is 1 cm for (a) and 2 cm for (b–e).

turned off in EXP2, the wind forcing is turned off in EXP3, and the closed SCS boundary is used in EXP4. Therefore, the individual influence of the buoyancy forcing, the wind forcing and the open boundary forcing on the northern SCS can be approximately isolated by subtracting EXP2,

EXP3 and EXP4 from the control run (EXP1), as illustrated in Figs. 6c–e.

The forced Rossby wave excited only by wind forcing (Fig. 6d) is very close to that in EXP1 (Fig. 6b), except that the former yields slightly weaker amplitudes and smaller horizontal scale of the forced wave. The propagation of this Rossby wave is also identical to that in EXP1 and observations, migrating northwestward to the Guangdong coast and then transforming into a Kelvin wave, propagating southward along the coast. The buoyancy forcing alone, however, cannot excite Rossby waves but rather causes a local oscillation in the SSH without any horizontal migration of the center (Fig. 6c). The buoyancy forced SSH anomaly, that is, the surface steric height anomaly, actually reflects the expansion/contraction of the water column in the mixed layer (Gill and Niiler, 1973; Liu et al., 2001). The open boundary forcing (Fig. 6e), in which the Kuroshio is the most important, can excite Rossby waves in the northern SCS, but with the amplitude (−6 cm) smaller than that in EXP1. This Rossby wave, instead of propagating northwestward to the Guangdong coast as shown in Figs. 6b and d, moves southwestward along the 1000 m isobath to the Vietnam coast. This experiment indirectly suggests that it is the migration of the wind stress curl anomaly that controls the evolution of the northern SCS SSH.

## 4. Vertical structure

The vertical structure of the forced Rossby wave shows that the winter LCE corresponds to a cold temperature anomaly that extends from the surface to 800 m depth. Fig. 7 shows the longitude (latitude)-depth section of the temperature anomaly for the winter LCE along 18.75°N (118.25°E). In the control run (Figs. 7a, e), the temperature anomaly contours are flat in the mixed layer but bend dramatically downward below 40 m depth between 116°–120°E (Fig. 7a) and 17°–20°N (Fig. 7e). This suggests that the LCE may be related to a strong upwelling, extending from 800 m depth to the bottom of mixed layer.

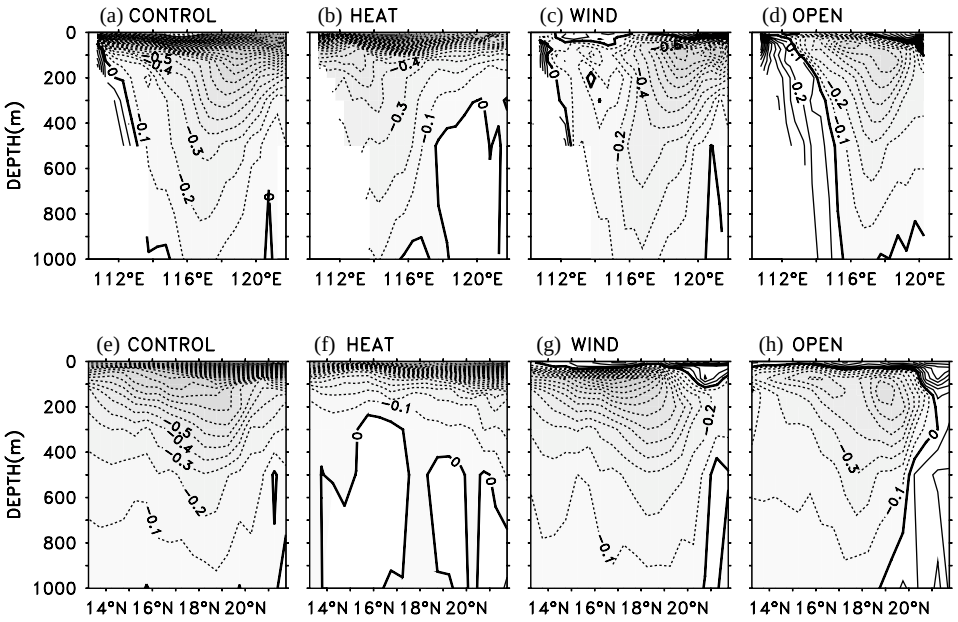


Fig. 7. The vertical section of the temperature anomalies relative to annual mean (CI = 0.1°C) along (a–d) 18.75°N and (e–h) 118.25°E in winter: (a), (e) the control run, (b), (f) the buoyancy forcing run, (c), (g) the wind forcing run and (d), (h) the open boundary forcing run.

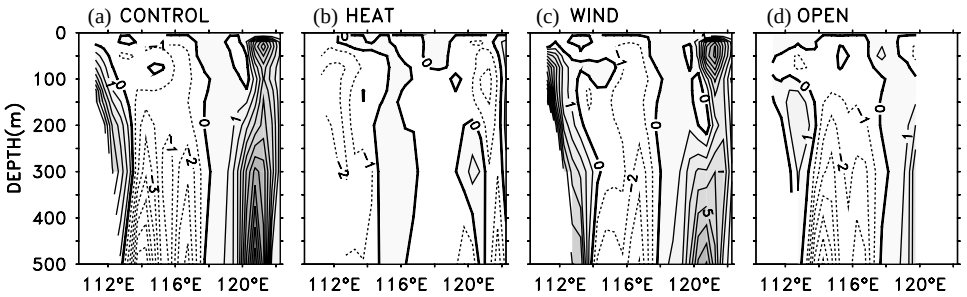


Fig. 8. The longitude-depth section of the vertical velocity along 18.75°N in winter. Solid (dashed) line represents upwelling (downwelling). CI is 1 m/day: (a) the control run, (b) the buoyancy forcing run, (c) the wind forcing run and (d) the open boundary forcing run.

Under the buoyancy-only forcing (Figs. 7b, f), no cold temperature anomaly is centered at the location of the LCE, because there is no Ekman pumping on the thermocline. In the case of wind-only forcing (Figs. 7c, g), the temperature pattern indicates that the upwelling can reach the surface. The vertical temperature structure in the case of boundary forcing (Figs. 7d, h) shows a smaller cold temperature anomaly, implying a weaker upwelling than in the control and wind forcing runs.

The zonal cross section of vertical velocity along 18.75°N (Fig. 8) shows features consistent with the temperature section (Fig. 7). The solid (dashed) lines represent upwelling (downwelling). In the control run (Fig. 8a), there is a continuous upwelling from at least 500 m to the mixed layer depth, with the maximum vertical velocity of over 10 m/day at 500 m depth, in the region of the LCE (117°–121°E). The upwelling rate above 200 m depth is about 5 m/day. The buoyancy forcing (Fig. 8b) cannot generate upwelling; instead, it causes downwelling in the LCE region, with a downwelling rate of about 2 m/day. The wind forcing (Fig. 8c) and the Kuroshio (Fig. 8d) cause upwelling with speeds of 7 and 3 m/day at 500 m depth, respectively.

## 5. Discussion and conclusion

The evolution of the SSH in the northern SCS can be seen as the evolution of a forced Rossby wave with an annual period, based on observations and the model. The forced Rossby wave originates the northwest off Luzon Island and propagates northwestward to the Guangdong coast with a speed of about 5 cm/s. The maximum horizontal scale of this wave is over 400 km. The negative phase of the forced Rossby wave in winter is associated with the LCE. It corresponds to a strong upwelling off Luzon Island with a maximum simulated upwelling rate of about 10 m/day at 500 m depth. Sensitivity experiments confirm that the wind stress curl dominates the occurrence and propagation of the forced Rossby wave, while the Kuroshio is of secondary importance. The buoyancy forcing cannot generate a propagating wave, but rather causes a local oscillation in the mixed layer depth.

The strength and the horizontal and vertical extension of the upwelling off Luzon Island in winter are found to be larger in the numerical experiments than those of the upwelling off the Pacific and Atlantic coasts (Pickard and Emery, 1990). For example, off the North American coast from British Columbia to California, the width of the upwelling zone is on the order of 100 km and the upwelling speed some 5–10 m/day. The relatively cool water comes from depths of no more than 300 m. Off the South American coast, upwelling originates at an average depth of 130 m, with a maximum of 350 m (Pickard and Emery, 1990). The stronger upwelling off Luzon Island might be the result of relatively small size of the SCS and relatively stronger external forcing. The combined effects of the positive wind stress curl in winter and the anticyclonic deformation of

the Kuroshio in the Luzon Strait (Liu and Liu, 1996) can generate strong positive potential vorticity northwest off Luzon Island and, as a result, a strong upwelling. The strong northern SCS upwelling in winter suggests that the upwelling may include cool water coming from the intermediate layer (500–1000 m) and even the deeper layer (below 1000 m). Therefore, this local winter upwelling, that is, the LCE, is probably connected to the basin-scale SCS thermohaline circulation (Shaw et al., 1996). As ventilation for the SCS thermohaline circulation, this upwelling may have important implications to the study of the SCS ecosystem (Chao and Shaw, 1996). Consequently, the future work will explore the possible connection between this upwelling and the basin-scale circulation using a higher resolution general circulation model.

## Acknowledgements

This work is supported by the NSF of China (49636230), the National Key Program for Developing Basic Science (G1999043807) and the NSFC Special program (40028605). The authors thank Editor, Dr. Michael Bacon and three anonymous reviewers for their valuable comments.

## References

Blumberg, A.F., Mellor, G.L., 1987. A description of a three-dimensional coastal ocean circulation model. In: Heaps, N. (Ed.), Three-dimensional Coastal Ocean Models, Vol. 4. American Geophysical Union, Washington, DC, pp. 208.

Chambers, D., Tapley, B., Stewart, R., 1997. Long-period ocean heat storage rates and basin-scale heat fluxes from TOPEX. Journal of Geophysical Research 102, 10525–10533.

Chao, S.Y., Shaw, P.T., 1996. Deep water ventilation in the South China Sea. Deep-Sea Research I 43 (4), 445–466.

Chu, P.C., Edmons, N.L., Fan, C., 1999. Dynamical mechanisms for the South China Sea seasonal circulation and thermohaline variabilities. Journal of Physical Oceanography 29 (11), 2971–2989.

da Silva, A., Young, C., Levitus, S., 1994a. Atlas of surface marine data 1994, Volume 1: algorithms and procedures. NOAA Atlas NESDIS 6. US Department of Commerce, NOAA, NESDIS.

Gill, A., Niiler, P., 1973. The theory of the seasonal variability in the ocean. Deep-Sea Research I 20, 141–177.

Guo, Z., 1988. The Kuroshio and mass transport in the Luzon Strait in September 1985. Tropical Oceanography 2, 13–19 (in Chinese).

Ho, C.R., Zheng, Q., Soong, Y.S., Kuo, N.J., Hu, J.H., 2000. Seasonal variability of sea surface height in the South China Sea observed with TOPEX/Poseidon altimeter data. Journal of Geophysical Research 105 (C6), 13981–13990.

Levitus, S., Boyer, T.P., 1994. World Ocean Atlas 1994 Volume 4: Temperature. NOAA Atlas NESDIS 4, 177pp.

Liu, Q., Liu, C., 1996. The deformation and dynamic mechanism of the Kuroshio Current in the Luzon Strait (in Chinese). Journal of Qingdao Ocean University 26 (4), 413–419.

Liu, Z., Yang, H.J., Liu, Q., 2001. Regional dynamics of seasonal variability of sea surface height in the South China Sea. Journal of Physical Oceanography 31 (1), 272–284.

Pickard, L., George, W.J.E., 1990. Descriptive Physical Oceanography: An Introduction, 5th Edition. Pergamon Press, Oxford, pp. 279–280.

Qu, T.D., 2000. Upper-layer circulation in the South China Sea. Journal of Physical Oceanography 30 (6), 1450–1460.

Shaw, P.T., Chao, S.Y., 1994. Surface circulation in the South China Sea. Deep-Sea Research I 41, 1663–1683.

Shaw, P.T., Chao, S.Y., Liu, K.K., Pai, S.C., Liu, C.T., 1996. Winter upwelling off Luzon in the Northeastern South China Sea. Journal of Geophysical Research 101 (C7), 16435–16448.

Shaw, P.T., Chao, S.Y., Fu, L., 1999. Sea surface height variations in the South China Sea from satellite altimetry. Oceanologica Acta 22, 1–17.

White, W.B., 2000. Tropical coupled Rossby waves in the Pacific ocean—atmosphere system. Journal of Physical Oceanography 30 (6), 1245–1264.

White, W.B., 2001. Evidence for coupled Rossby waves in the annual cycle of the Indo–Pacific ocean. Journal of Physical Oceanography 31 (10), 2944–2957.

Wyrtki, K., 1961. Physical oceanography of the Southeast Asia waters. NAGA Report 2, 1–195.

Yang, H.J., Liu, Q., 1998. Seasonal features of the temperature distribution in the upper layer of the South China Sea. Oceanography and Limnology 29 (5), 501–507 (in Chinese).

Yang, H.J., Liu, Q., Liu, Z., Wang, D.X., Liu, X.B., 2002. A GCM study of the dynamics of the upper ocean circulation of the South China Sea. Journal of Geophysical Research 107(C7), doi:10.1029/2001JC001084.